Stress-Strain Characteristics of Reinforced Concrete in Pure Shear

Les relations tensions-déformations du beton armé soumis au cisaillement pur

Spannungsdehnungsverhalten von Stahlbeton unter reinem Schub

F. VECCHIO
Doctoral Student
University of Toronto
Toronto, Canada

M.P. COLLINS
Professor
University of Toronto
Toronto, Canada

SUMMARY
Experiments in which reinforced concrete panels were loaded in pure shear are described. It is shown that the observed behaviour of the panels can be predicted by using basis equilibrium and compatibility conditions in addition to appropriate stress-strain relationships for the concrete and the steel.

RÉSUMÉ
Des essais sont décrits concernant des panneaux en béton armé soumis au cisaillement pur. On démontre que le comportement des panneaux, tel qu'observé, peut être prédit en utilisant les conditions usuelles d'équilibre et de compatibilité, en plus des relations appropriées entre contraintes et déformations unitaires pour le béton et l'acier.

ZUSAMMENFASSUNG
Versuche, in denen Stahlbetonscheiben nur mit Schubkräften belastet werden, werden beschrieben. Es wird gezeigt, dass man das beobachtete Verhalten der Scheiben durch die Benützung von elementarem Gleichgewicht und Verträglichkeitsbedingungen wie auch von geeigneten Spannungs-Dehnungs Linien für Beton und Stahl beschreiben kann.

1. INTRODUCTION

Developing a rational theory capable of predicting the behaviour of reinforced concrete subjected to shear has been the goal of a large number of research engineers for very many years. Achieving this goal would enable current empirical shear design procedures to be replaced by methods comparable in rationality and generality to the procedures now used in the design of reinforced concrete for flexure and axial load.

In the past many researchers have tackled the shear problem by testing simply supported beams subjected to point loads. A fundamental difficulty inherent in such tests is that no substantial region of the specimen is subjected to uniform stress conditions. The local disturbances caused by the point loads and the reactions plus the changing moments along the span mean that (apart from end-to-end symmetry) no two points on the specimen behave in quite the same manner.

It is the authors' belief that before we can understand the behaviour of reinforced concrete in complex load situations involving shear we must first understand its behaviour in pure shear. Hence, as part of an ongoing research programme at the University of Toronto [1], an experimental project in which reinforced concrete elements were loaded in pure shear was undertaken. This paper will describe the preliminary results of this "pure shear" project.

2. LOADING REINFORCED CONCRETE IN PURE SHEAR

The test specimens were concrete panels, 890 mm square by 70 mm thick, reinforced with two layers of welded wire fabric, Fig. 1. Five steel shear keys, anchored with shear studs, were cast into each edge of the specimen.

The specimens were loaded via links pinned to the steel shear keys. Each key was acted upon by two inclined links, one at +45° to the normal to the specimen edge and the other at -45°, Fig. 2. When one link pulled, while the other pushed with the same force, a resultant force parallel to the edge of the specimen was produced.
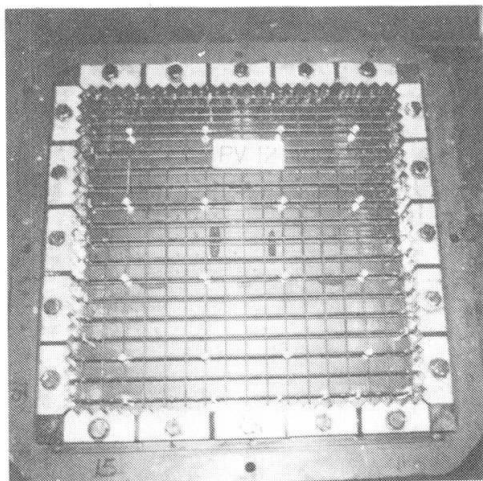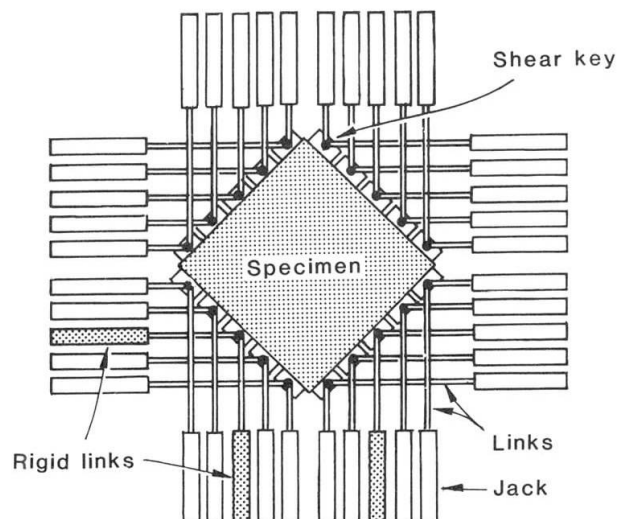

Fig. 1 Specimen Ready for Casting

Fig. 2 Hydraulic Jack and Link Assembly

The forces in the 40 links (2 x 5 x 4) were produced by 37 double-acting hydraulic jacks acting on 37 of the links. The remaining three links were fixed in length in order to stabilize the overall position of the specimen within the rig.

To prevent out-of-plane movement of the panel the shear keys were attached to an auxiliary frame by means of tie-rods with spherical rod ends, Fig. 3.
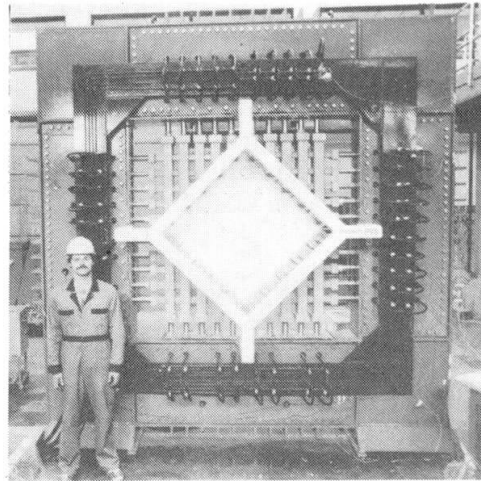

Fig. 3   Rear View of Shear Rig

3.   DESCRIPTION OF SPECIMENS

Table 1 summarizes the parameters of the 17 specimens tested to date. The pure shear tests were subdivided into two groups. In the Series I tests, the amount of reinforcing was varied; but, for a given specimen, the amount of reinforcing in the transverse direction was always equal to that in the longitudinal direction (longitudinal and transverse were defined as directions parallel to the edges of the specimen, Fig. 1). For the Series II tests, the amount of reinforcing in the longitudinal direction was held constant while the transverse reinforcement was varied. The two panels of Series III were tested in uniaxial compression to calibrate the performance of the test set-up.

TABLE 1.   SPECIMEN PARAMETERS

| Specimen	Percentage of Steel Reinforcement		Steel Yield Strength (MPa)		Concrete Strength	Cylinder Strain at Peak
	Long.	Trans.	Long.	Trans.	f'_c (MPa)	ϵ_o (x10^{-3})
Series I						
PV2	0.18	0.18	430	430	23.5	2.25
PV3	0.48	0.48	660	660	26.6	2.30
PV16	0.74	0.74	250	250	21.7	2.00
PV5	0.74	0.74	620	620	28.3	2.50
PV4	1.06	1.06	240	240	26.6	2.50
PV14	1.79	1.79	460	460	20.4	2.23
PV6	1.79	1.79	270	270	29.8	2.50
PV7	1.79	1.79	450	450	31.1	2.50
PV8	2.62	2.62	460	460	29.8	2.50
Series II						
PV13	1.79	–	250	–	18.2	2.70
PV12	1.79	0.45	470	270	16.0	2.50
PV10	1.79	1.00	280	280	14.5	2.70
PV11	1.79	1.31	240	240	15.6	2.60
PV1	1.79	1.68	480	4£0	34.5	2.20
PV9	1.79	1.79	460	460	11.6	2.80
Series III						
PV15	0.74	0.74	250	250	21.7	2.00
PV17	0.74	0.74	250	250	20.4	2.00

Brass strain targets were fixed onto the reinforcing steel and protruded to the surfaces of the specimen. Sixteen targets, on a 200 mm grid, were used on each side of the specimen.

Strains were read (using a demountable mechanical strain gauge) in the longitudinal, transverse, and the two diagonal (+45° and -45°) directions; resulting in a total of 84 separate readings.

4. TESTING OF THE SPECIMENS

In the Series I tests, the initial cracks formed at 45° to the steel grid at a shear stress of approximately $0.33 \sqrt{f_c'}$ (MPa). As the load increased the number and width of the cracks also increased, but the direction of the cracks did not change. Failure occurred either by a mass yielding of the steel, Fig. 4, or by a sliding shear failure of the concrete, Fig. 5. The mode of failure depended on the amount and strength of the reinforcing relative to the concrete. The ultimate shear stress, as a fraction of f_c', increased with the percentage of reinforcing. The maximum shear stress attained was $0.32 f_c'$.
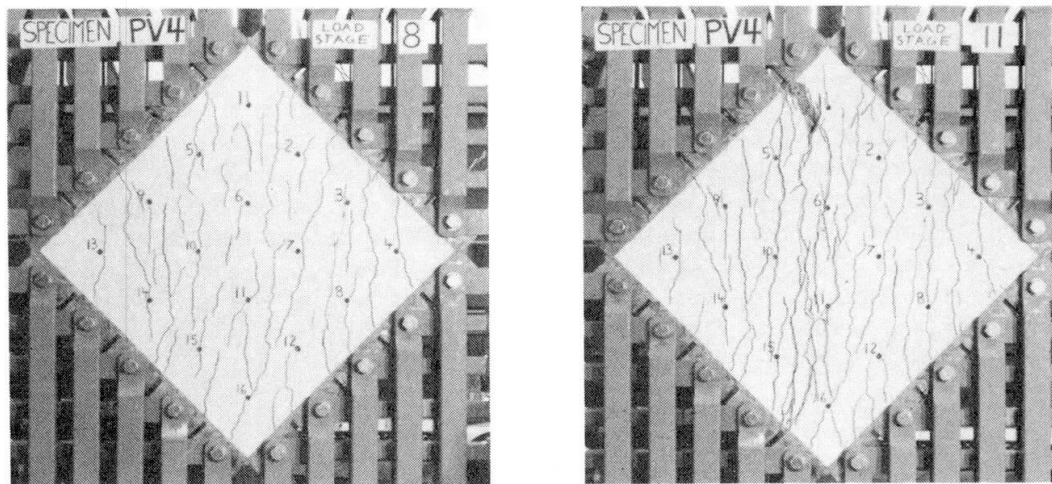
(a) Prior to yielding, v = 2.40 MPa   (b) Yielding at v = 2.89 MPa

Fig. 4   Specimen PV4: Steel Yielding Failure

In the Series II tests, the initial cracks also formed at 45°. In this case, however, as the load increased the cracks began to shift direction to become more acute to the longitudinal steel direction, Fig. 6. Failure at ultimate occurred either by: (i) yielding of both the transverse and longitudinal steel; (ii) sliding shear failure of the concrete after the transverse steel had yielded but prior to the yielding of the longitudinal steel, or (iii) sliding shear failure of the concrete prior to yielding of the transverse steel. The mode of failure and ultimate shear strength was influenced mostly by the percentage and strength of the transverse reinforcing.
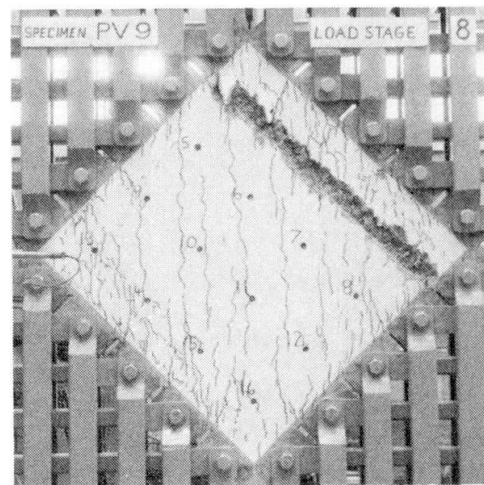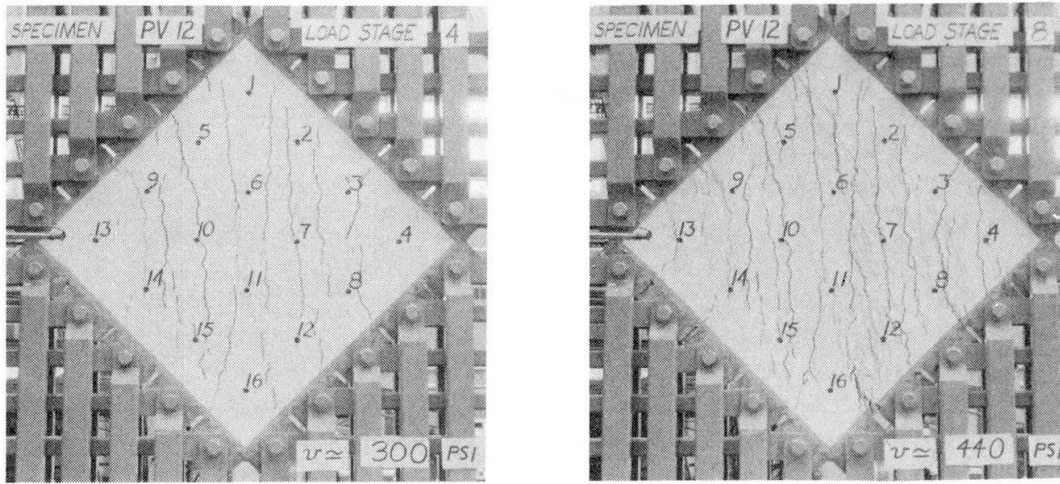

Fig. 5   Specimen PV9: Sliding Shear Failure of Concrete

(a) Shortly after cracking, v = 2.1 MPa   (b) At ultimate, v = 3.13 MPa

Fig. 6   Specimen PV12: Cracks Shifting Direction

One specimen tested, PV2, was under-reinforced in both directions. It failed immediately after the formation of the diagonal cracks, Fig. 7.
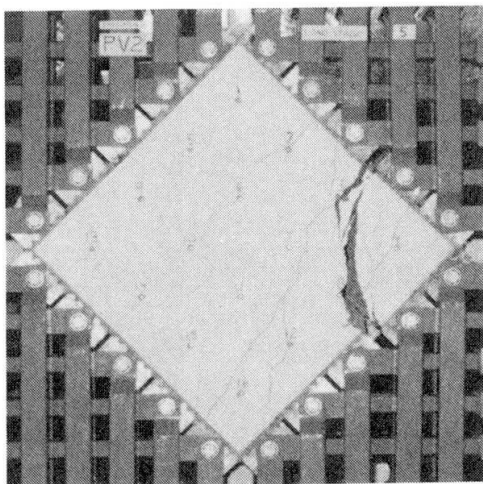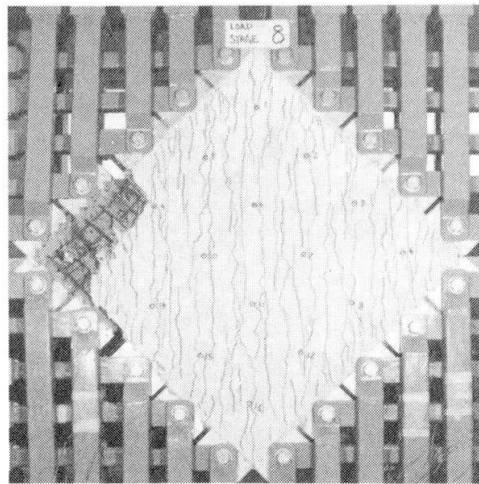

Fig. 7   Specimen PV2: Failure of Under-   Fig. 8   Specimen PV1: Premature Failure
         reinforced Panel Upon First   Due to "Pull-Out" of Shear Keys
         Cracking

Unfortunately, some of the test specimens failed prematurely due to a local pull-out failure of the shear keys, Fig. 8. These occurred mostly in the earlier tests where a uniform concrete mix was used throughout the specimen. In later tests, a band of strong concrete was used in the peripheral areas to help alleviate the load transfer problem. A summary of the cracking stresses, ultimate stresses, and mode of failure is given in Table 2.

The two specimens of Series III were tested in uniaxial compression applied in the longitudinal direction. The test on specimen PV15 had to be halted prior to failure because the applied load was approaching the capacity of the rig and a leak had developed in the hydraulic system resulting in severe pressure losses.

TABLE 2:   TEST OBSERVATIONS

Specimen	V_{cr} (MPa)	V_u (MPa)	Mode of Failure
PV 1	2.21	8.00	Pull-out
PV 2	1.10	1.16	Cracking [1]
PV 3	1.66	3.07	Steel rupture [2]
PV 4	1.79	2.89	Yielding
PV 5	1.73	4.24	Pull-out
PV 6	2.00	4.55	Local yielding
PV 7	1.93	6.81	Pull-out
PV 8	1.73	6.67	Pull-out
PV 9	1.38	3.74	Concrete shear
PV 10	1.86	3.97	Concrete shear
PV 11	1.66	3.56	Local yielding
PV 12	1.73	3.13	Concrete shear
PV 13	1.73	2.01	Concrete shear
PV 14	1.93	5.24	Pull-out
PV 16	2.07	2.14	Yielding

1   Initially cracked at 90°
2   Non-stress relieved wires ruptured at welds, Fig 9

With Specimen PV17, loading proceeded to failure. At ultimate, there was an ex-
plosive failure of the concrete, Fig. 10, with large pieces of concrete thrown
as far as 20 m. Prior to failure, only one or two small longitudinal cracks were
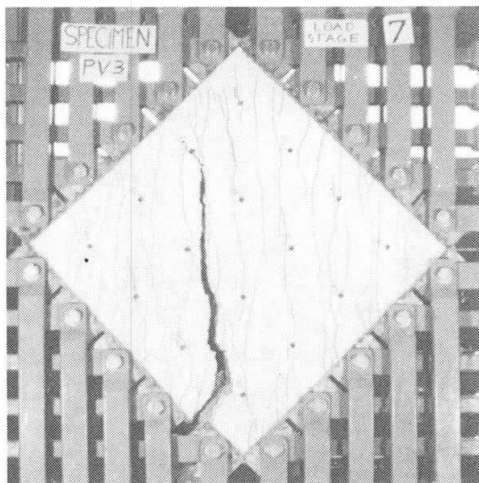visible.

Fig. 9   Specimen PV3: Brittle Failure   Fig. 10   Specimen PV17: Explosive Failure
          Due to Fracture of Steel   of Panel in Uniaxial Compression

At ultimate, the concrete compressive stress in PV17 reached 1.04 f'_c.

5.   ANALYSIS OF TEST DATA

The data gathered from a particular specimen was analyzed such that Mohr's
circles of stress and strain could be drawn at every load stage.

The strain readings were reduced to average strains in the longitudinal, trans-
verse, + 45° diagonal and − 45° diagonal directions; ε_ℓ, ε_t, ε_{+45} and ε_{-45}

respectively. These strains were used to define a Mohr's circle of average strains, Fig. 11. Since four separate items of information were being used to define a circle, there existed one redundant point. The fact that all four points lay very close to it inspired confidence in the accuracy of the strain data.

Defining the strain circle fixed the values of: (i) the principal compressive strain, ε_d; (ii) the principal tensile strain, ε_{dt}; (iii) the normal shear strain, $\gamma_{\ell t}$; (iv) the maximum shear strain, γ_m; and (v) the angle of inclination of the principal compression, θ'.

From the strains in the longitudinal and transverse directions, the average steel tensile stresses ($f_{s\ell}$ and f_{st}) were determined from the stress-strain relationship of the reinforcement. These steel stresses, in turn, permitted the average concrete compressive stresses in the longitudinal and transverse directions, f_ℓ and f_t, respectively, to be calculated ($f_\ell = \rho_\ell f_{s\ell}$ and $f_t = \rho_t f_{st}$). Given the applied shear stress, v, and the calculated concrete stresses f_ℓ and f_t, the Mohr's circle of concrete stress could be drawn, Fig. 12. From the stress circle, the principal compressive stress, f_d, and principal tensile stress, f_{dt}, in the concrete were found.
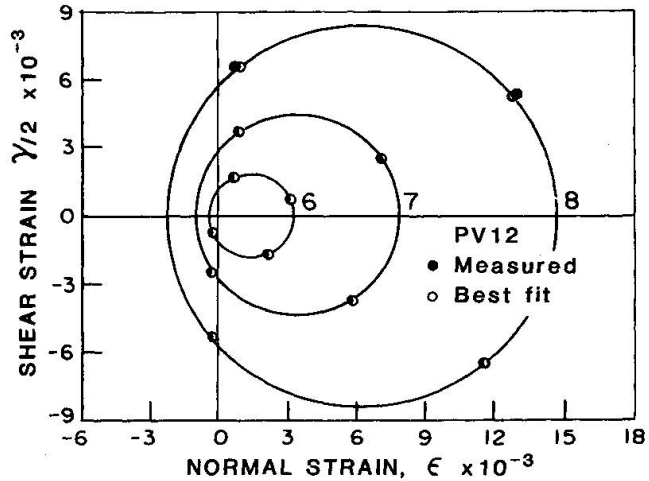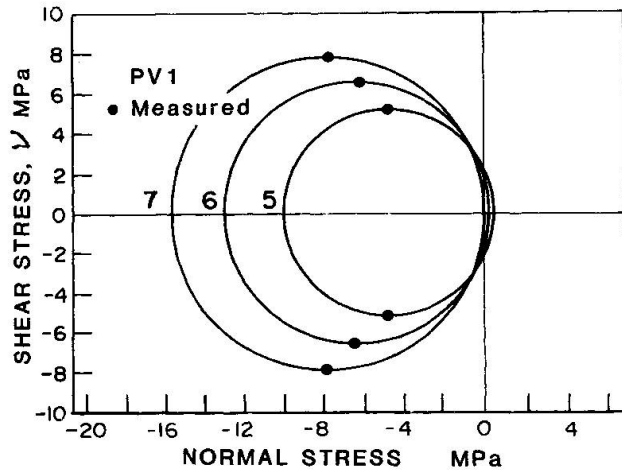

Fig. 11   Mohr's Circles of Strain for Specimen PV12

Fig. 12   Mohr's Circles of Stress for Specimen PV1

6. STRESS-STRAIN CHARACTERISTICS OF THE CONCRETE IN COMPRESSION

In Fig. 13, the observed relationships between principal compressive stress and principal compressive strain are shown for four of the panels. It can be seen that the principal compressive stress is not solely a function of the principal compressive strain. As has been previously suggested [2], it would appear that these relationships are influenced by the magnitude of the maximum co-existing shear strains, γ_m.

To further investigate the effects of shear strain, separate plots of the $f_d : \varepsilon_d$ data were made for specific
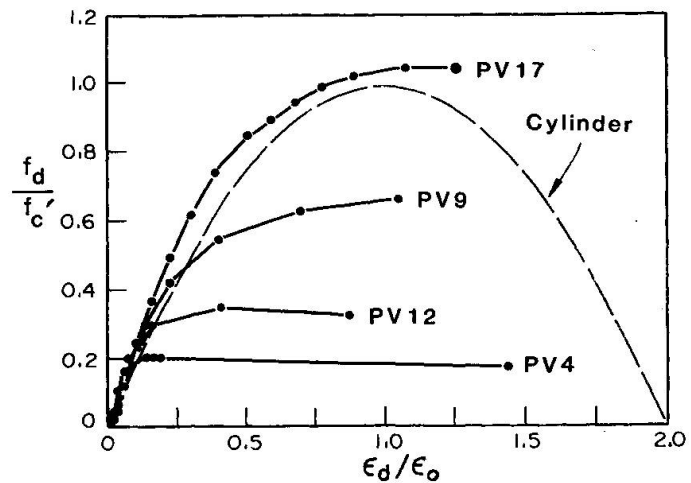

Fig. 13   Principal Compressive Stress vs. Principal Compressive Strain

ranges of the ratio γ_m/ε_d (see Fig. 14). It could be concluded that shearing strains had a degrading effect on the compressive stress-strain response of concrete. Furthermore, the magnitude of this effect appeared related to the ratio of maximum shear strain to principal compressive strain, γ_m/ε_d.
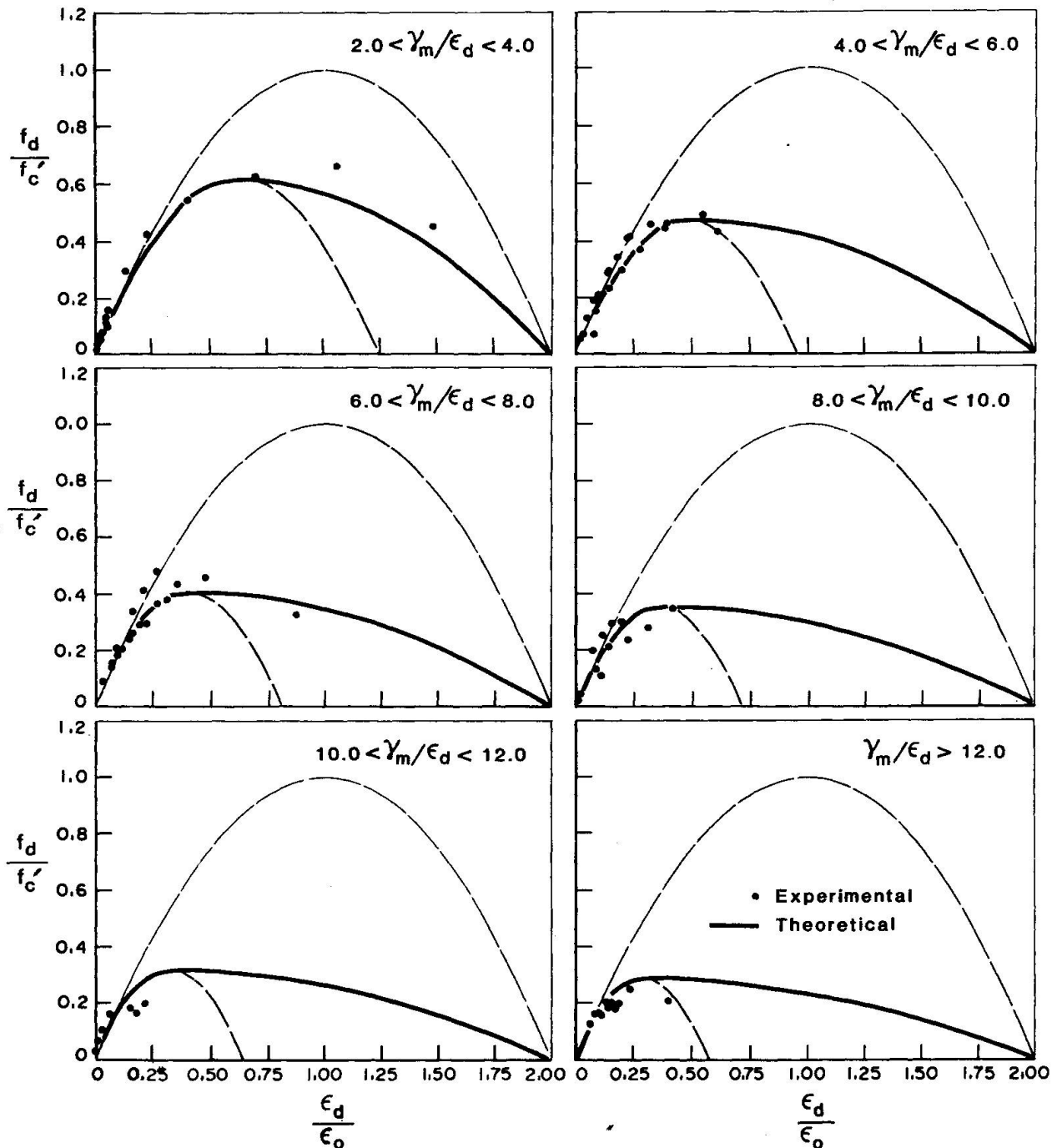
Fig. 14 Influence of Shear Strain on Principal Compressive Stress-Strain

An expression was derived to model the observed behaviour. It involved the addition of a modifying term in the commonly used parabolic stress-strain curve for concrete. The modified expression was:

$$f_d = f_c' \left[2 \left(\frac{\varepsilon_d}{\varepsilon_o}\right) - \lambda \left(\frac{\varepsilon_d}{\varepsilon_o}\right)^2 \right] \qquad \dots (1)$$

where

$$\lambda = (\gamma_m/\varepsilon_d - \mu)^{0.5} \qquad \dots (2)$$

Poisson's ratio, μ, is taken equal to 0.30; a value commonly observed near failure in concrete cylinders. The term 'λ' degenerates to 1.0 in the case of uniaxial compression, leaving the customary parabolic curve passing through (ε_o, f'_c).

For a given ratio of γ_m/ε_d, the peak concrete compressive stress attainable, f_p, is:

$$f_p = f'_c/\lambda \qquad \ldots (3)$$

The strain at which this peak stress is achieved, ε_p, is:

$$\varepsilon_p = \varepsilon_o/\lambda \qquad \ldots (4)$$

Thus, all peak stresses for various values of γ_m/ε_d lie on the line passing through the points (0, 0) and (ε_o, f'_c).

The experimental $f_d{:}\varepsilon_d$ data indicated that the concrete had considerably more ductility after peak strain than that predicted by Eq.(1). Thus, a more gradual unloading portion of the stress-strain curve was required. This was achieved by a transition curve between Eq.(1) and the usual parabolic expression, after peak stress.

In summary, given the principal compressive strain (ε_d) and the maximum shear strain (γ_m), the principal compressive stress (f_d) can be determined as follows:

(i) Determine shear strain coefficient, λ:

$$\lambda = (\lambda_m/\varepsilon_d - 0.3)^{0.5} \qquad \ldots (5)$$

(ii) Determine peak stress and peak strain, f_p and ε_p respectively:

$$f_p = f'_c/\lambda \qquad \ldots (6)$$

$$\varepsilon_p = \varepsilon_o/\lambda \qquad \ldots (7)$$

(iii) If $\varepsilon_d \leq \varepsilon_p$:

$$f_d = f'_c \left[2(\frac{\varepsilon_d}{\varepsilon_o}) - \lambda(\frac{\varepsilon_d}{\varepsilon_o})^2 \right] \qquad \ldots (8)$$

(iv) If $\varepsilon_d > \varepsilon_p$:

$$f_d = f_p \cdot (1 - \eta^2) \qquad \ldots (9)$$

where

$$\eta = \frac{(\varepsilon_d - \varepsilon_p)}{(2\varepsilon_o - \varepsilon_p)} \qquad \ldots (10)$$

The correlation between the test data and the prediction model was quite good (see Fig. 14). A coefficient of variation of 16% was obtained for points where f_d/f'_c was greater than 0.15.

7. STRESS-STRAIN CHARACTERISTICS OF CONCRETE IN TENSION

The stress circles determined for each of the pure shear test specimens showed that the concrete continued to carry some average tensile stresses even after cracking. These stresses, which are the result of the tensile stresses in the concrete between the cracks, must be less than the tensile cracking strength of the concrete, f_{cr}, but are significantly greater than zero, Fig. 15.

While equilibrium relationships are written in terms of average stresses, it will still be necessary for the reinforcement to transmit the loads across the cracks. At these locations tensile stresses in the concrete cannot assist the
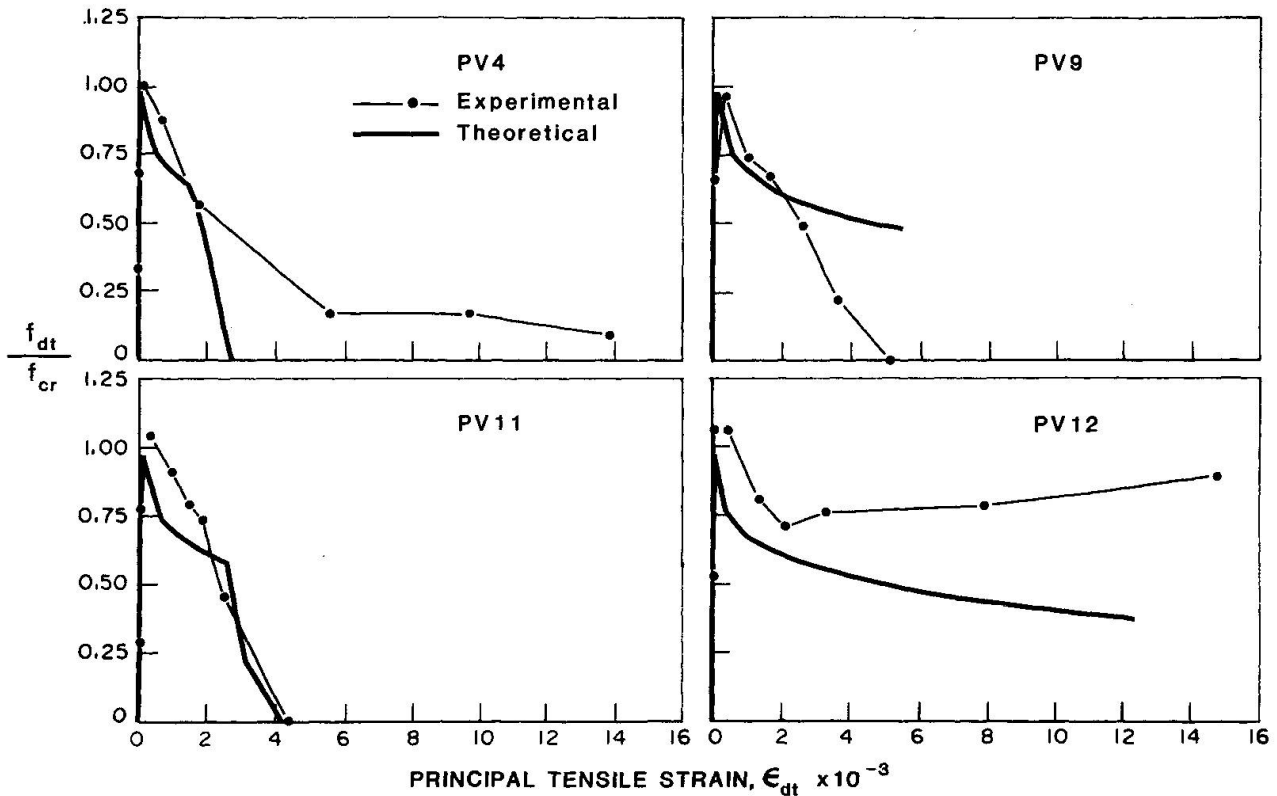
Fig. 15 Principal Tensile Stress-Strain Behaviour of Concrete

reinforcement. Hence, when the average stresses in the reinforcement approach yield, the average tensile stresses in the concrete are assumed to approach zero.

Based on the observed behaviour of the panels, the following procedure is suggested for calculating the average principal tensile stress, f_{dt}, from the average principal tensile strain, ε_{dt}.

(i)   Prior to cracking:

$$f_{dt} = (\varepsilon_{dt} - 0.15 \, \varepsilon_d) \cdot E_c \leq f_{cr}$$

$$\text{where} \quad E_c = \frac{2f_c'}{\varepsilon_o} \quad \text{and} \quad f_{cr} = 0.33 \sqrt{f_c'(\text{MPa})}$$

(ii)   After cracking:

$$f_{dt} = f_{cr} \frac{1}{1 + (\frac{\varepsilon_{dt}}{.005})^{0.5}}$$

$$\leq \rho_\ell (f_{s\ell y} - f_{s\ell}) \sin^2\theta + \rho_t (f_{sty} - f_{st}) \cos^2\theta$$

It can be seen from Fig. 15 that the predictions of the above model follow the trend of the experimental data. However, as might be expected for a phenomenon dependent on the tensile strength of the concrete and the bond characteristics of the reinforcement, there is considerable scatter in the data. Fortunately, the tensile stresses are only a small component of the total stress circle (Fig. 12). Hence, large errors in the predicted tensile stress will not necessarily result

in large errors in the predicted behaviour. It is, however, necessary to include the contribution of the concrete tensile stresses if accurate predictions of deformation at all stages of loading are to be made.

8.   PREDICTING THE RESPONSE OF THE PANELS

The complete shear response of the reinforced concrete elements can be traced by solving for stress and strain conditions as the principal compressive strain, ε_d, is incremented.

For a given value of ε_d, solving for all stress and strain requirements involves an iterative procedure. Two other strain conditions, typically ε_ℓ and θ, must be estimated. Conditions of equilibrium and compatibility are checked, and the estimates adjusted accordingly, until convergence is achieved.

A schematic representation of this solution procedure is given in Fig. 16. A detailed, step by step description follows.

Step 1:   Choose value of principal compressive strain, ε_d.

Step 2:   Estimate longitudinal strain, ε_ℓ.

Step 3:   Estimate angle of inclination of principal compressive strain, θ'.

Fig. 16   Solution Procedure for Pure Shear Response of Reinforced Concrete Element

Step 4:   Determine all other strain conditions from the circle of strain, Fig. 17:

(i)   Normal shear strain $\gamma_{\ell t}$:

$$\gamma_{\ell t} = \frac{2 \, (\varepsilon_\ell + \varepsilon_d)}{\tan\theta'}$$

(ii)   Transverse steel strain, ε_t:

$$\varepsilon_t = \frac{\gamma_{\ell t}}{2 \, \tan\theta'} - \varepsilon_d$$

(iii)   Principal tensile strain, ε_{dt}:

$$\varepsilon_{dt} = \varepsilon_\ell + \varepsilon_t + \varepsilon_d$$

(iv)   Maximum shear strain, γ_m:

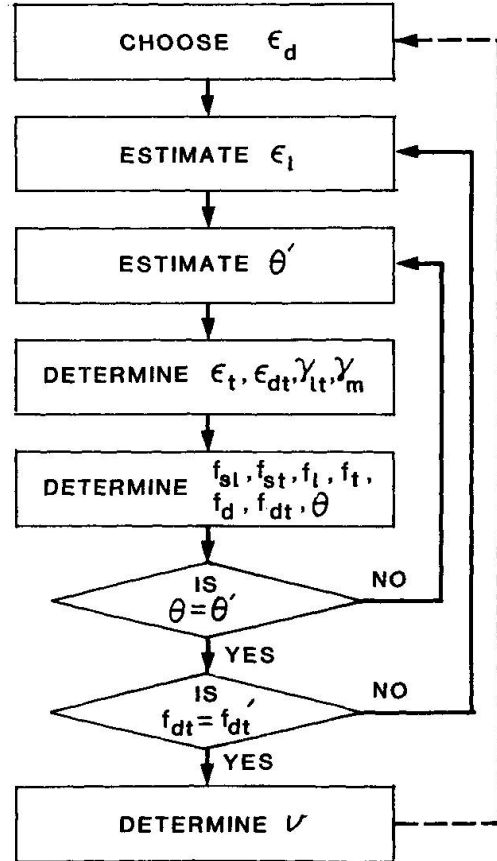$$\gamma_m = \varepsilon_t + \varepsilon_\ell + 2\varepsilon_d$$

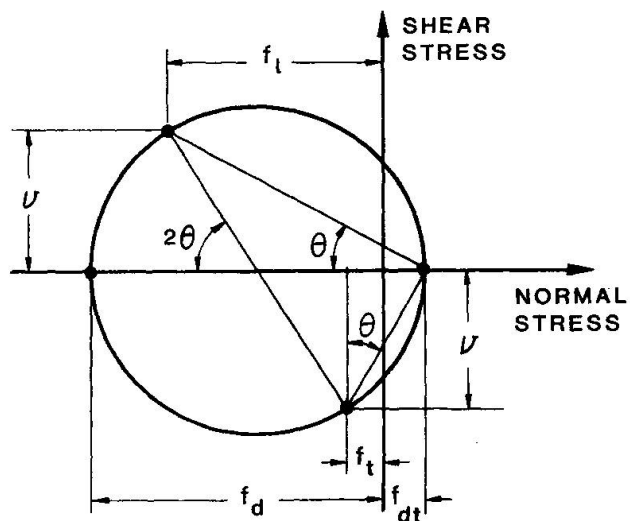

Fig. 17   Equilibrium Conditions for Average Stresses in Concrete

Step 5:   Determine stress conditions:

(i)   Longitudinal steel tensile stress, $f_{s\ell}$:

$$f_{s\ell} = \varepsilon_\ell \cdot E_s \leq f_{s\ell y}$$

(ii)   Transverse steel tensile stress, f_{st}:

$$f_{st} = \varepsilon_t \cdot E_s \leq f_{sty}$$

(iii)   Longitudinal concrete compressive stress, f_ℓ:

$$f_\ell = \rho_\ell \cdot f_{st}$$

(iv)   Transverse concrete compressive stress, f_t:

$$f_t = \rho_t \cdot f_{st}$$

(v)   Concrete principal compressive stress, f_d:

$$\lambda = (\gamma_m / \varepsilon_d - 0.3)^{0.5}$$

$$\varepsilon_p = \varepsilon_0 / \lambda$$

$$f_p = f_c' / \lambda$$

$$\eta = (\varepsilon_d - \varepsilon_p) / (2\varepsilon_0 - \varepsilon_p)$$

- If $\varepsilon_d \leq \varepsilon_p$, then

$$f_d = \left[2(\frac{\varepsilon_d}{\varepsilon_0}) - \lambda(\frac{\varepsilon_d}{\varepsilon_0})^2 \right]$$

- If $\varepsilon_d > \varepsilon_p$, then

$$f_d = f_p \cdot [1.0 - \eta^2]$$

(vi)   Concrete principal tensile stress, f_{dt}':

$$f_{cr} = 0.33 \sqrt{f_c'} \ (MPa)$$

$$E_c = 2 f_c' / \varepsilon_0$$

Prior to cracking:

$$f_{dt}' = E_c \cdot (\varepsilon_{dt} - 0.15 \, \varepsilon_d) \leq f_{cr}$$

After cracking:

$$f_{dt}' = f_{cr} / [1 + (\frac{\varepsilon_{dt}}{0.005})^{0.5}]$$

but $f_{dt}' < \rho_\ell (f_{s\ell y} - f_{s\ell}) \sin^2\theta' + \rho_t (f_{sty} - f_{st}) \cos^2\theta'$

(vii)   Angle of inclination of principal compressive stress, θ:

From stress circle, Fig. 18,

$$\theta = \tan^{-1} \left[\sqrt{\frac{f_d - f_\ell}{f_d - f_t}} \right]$$

Step 6:   Check compatibility:

Is $\theta = \theta'$?

If yes, go to step 7.
If no, go to step 3.

Step 7:   Check equilibrium:

From stress circle, Fig. 18,

$$f_{dt} = f_d - f_\ell - f_t$$

Is $f_{dt} = f_{dt}'$?

If yes, go to step 8.
If no, go to step 2.

Step 8:   Determine shear stress, v,
          from stress circle, Fig. 18,

$$v = (f_d - f_t) \cdot \tan\theta$$

Step 9:   Increment ε_d and repeat.

$$0 < \varepsilon_d \leq 1.5\,\varepsilon_o$$

$$\Delta\varepsilon_d \approx 0.05\,\varepsilon_o \text{ to } 0.10\,\varepsilon_o.$$
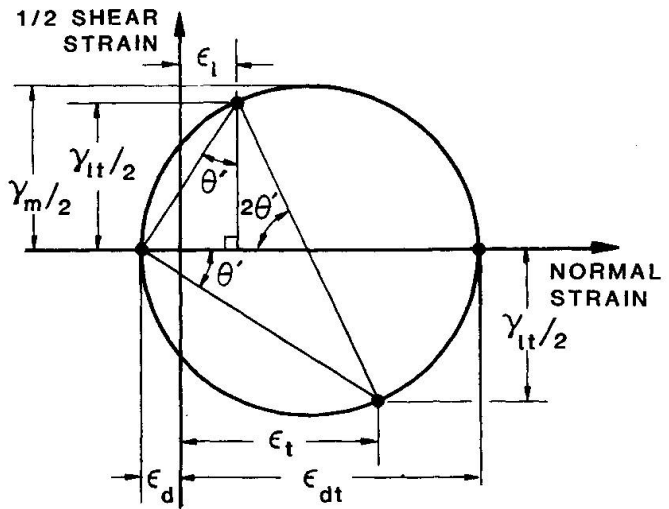

Fig. 18   Compatibility Conditions for
          Average Strains in Concrete

The above procedure was used to predict the response of the 15 panels loaded in
shear.   The resulting predicted shear stress – shear strain relationships for
these panels are compared with the experimentally determined response in
Fig. 19.   It can be seen that the theoretical predictions agree well with the
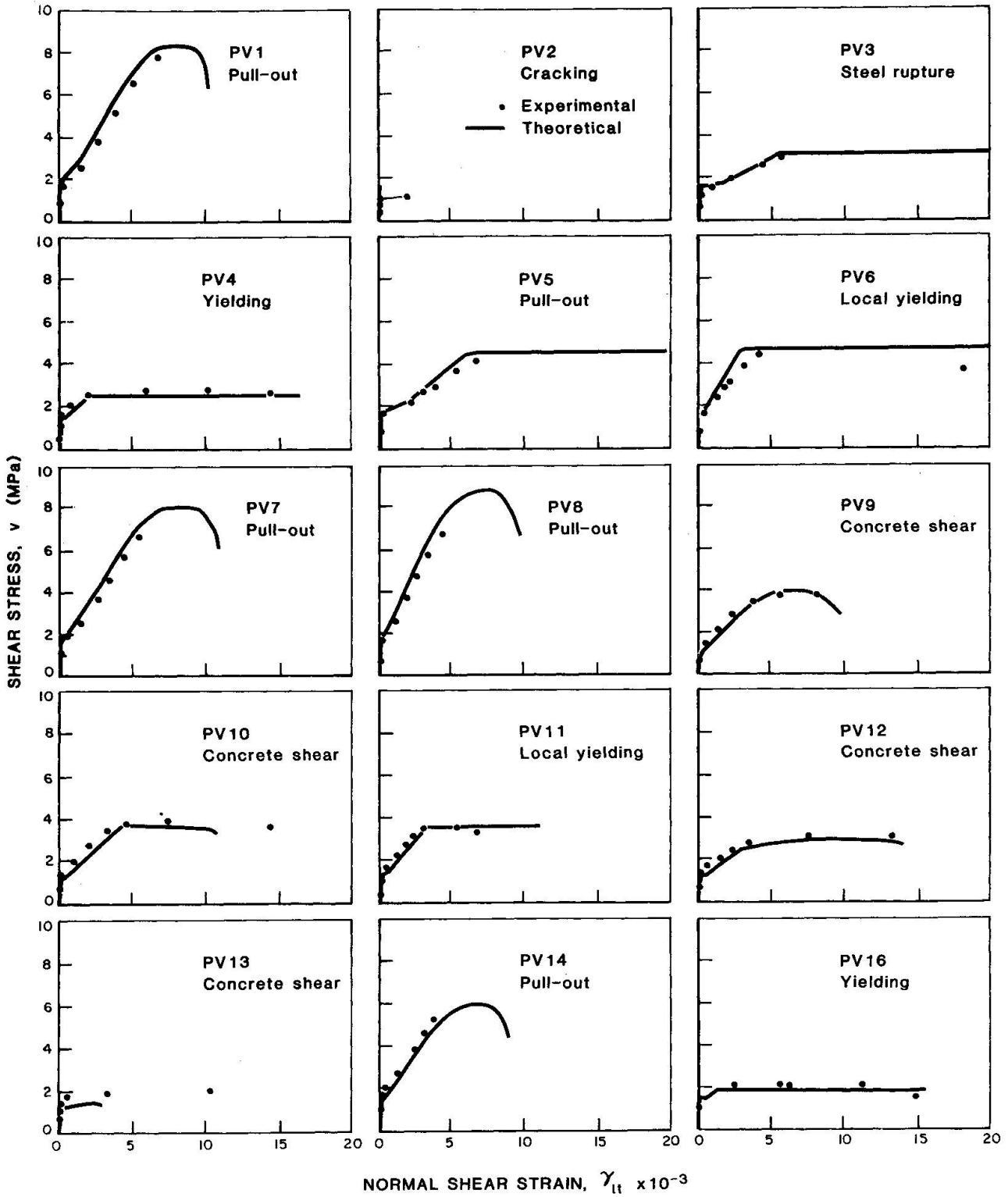experimental observations.

Fig. 19   Shear Stress – Shear Strain Response of 15 Specimens Tested

9. CONCLUDING REMARKS

The results of the 17 panels tested to date have demonstrated that the relation-
ship between the principal compressive stress in the concrete and the principal
compressive strain in the concrete is strongly dependent on the co-existing maxi-
mum shear strain. Further, it has been found that in order to predict accurately
the deformation characteristics of the panel, it is necessary to account for the
tensile stresses in the concrete.

Mathematical models were developed to represent the concrete stress-strain char-
acteristics. Using these models, equilibrium conditions based on average
stresses, and compatibility conditions based on average strains, it proved pos-
sible to predict accurately the behaviour of the panels.

Experimental work currently underway is aimed at investigating the applicability
of the models to more complex stress combinations, specifically combined tension
and shear, and combined compression and shear. Studies on the influence of re-
versed cyclic loading are also planned. Hopefully, the material properties de-
termined in this study can be incorporated into general mathematical models
which will enable complex reinforced concrete structures to be designed for shear
in a rational manner.

10. ACKNOWLEDGEMENT

11. REFERENCES

1. Collins, M.P.: "Reinforced Concrete Members in Torsion and Shear",
   IABSE Colloquium on Plasticity in Reinforced Concrete, Copenhagen,
   May 1979, pp. 119-130.

2. Collins, M.P.: "Investigating the Stress-Strain Characteristics of
   Diagonally Cracked Concrete", IABSE Colloquium on Plasticity in
   Reinforced Concrete, Copenhagen, May 1979, pp. 27-34.

Leere Seite

Blank page

Page vide